Chapter 5
Optical Characterization of Thin Films by Means of Imaging Spectroscopic Reflectometry

Miloslav Ohlídal, Jiří Vodák and David Nečas

Abstract This chapter focuses on optical characterization of thin films by means of non-microscopic imaging spectroscopic reflectometry. This technique is primarily intended for characterization of thin films with an area non-uniformity in their optical properties. An advantage of the technique is the possibility to measure along a relatively large area of the measured films. The motivation for development and exploitation of this technique is also discussed. Essential features and implementation of the technique are given, as well as the basic experimental set-up of imaging spectroscopic reflectometers and the way the experimental data are obtained. The data processing methods are classified based on the purpose of the thin film measurement. Furthermore, this chapter presents examples of results of imaging spectroscopic reflectometry in the field of thin films. At the end of the chapter, potential applications of imaging spectroscopic reflectometry in other tasks are also briefly mentioned.

M. Ohlídal (✉) · J. Vodák
Institute of Physical Engineering, Brno University of Technology,
Technická 2, 61669 Brno, Czech Republic
e-mail: ohlidal@fme.vutbr.cz

M. Ohlídal
Institute of Physics, Faculty of Mining and Geology,
VŠB-Technical University of Ostrava, Ostrava, Czech Republic

J. Vodák
Department of Physical Electronics, Masaryk University,
Kotlářská 267/2, 61137 Brno, Czech Republic
e-mail: jiri.vodak@yahoo.com

J. Vodák
Czech Metrology Institute, Okružní 31, 63800 Brno, Czech Republic

D. Nečas
Plasma Technologies, CEITEC, Masaryk University, Purkyňova 123,
61200 Brno, Czech Republic
e-mail: yeti@physics.muni.cz

© Springer International Publishing AG 2018

O. Stenzel and M. Ohlídal (eds.), *Optical Characterization of Thin Solid Films*, Springer Series in Surface Sciences 64,
https://doi.org/10.1007/978-3-319-75325-6_5

5.1 Introduction

The production of thin films and thin film systems, which possess novel and sophisticated properties desirable in optical applications, requires increasingly advanced techniques measuring these properties. In the following paragraphs, we will present one of such techniques, the imaging spectroscopic reflectometry (ISR) technique. We will describe the essential features and possibilities of the technique and also its implementation. We will classify the ISR methods and also we will demonstrate selected results achieved by means of them in the field of thin film optical characterization. It should be noted that we will differentiate between the concepts 'technique' and 'method' in the following text. We will use the expression 'technique' when referring to the way of obtaining experimental data. The expression 'method' will be used when describing the determination of thin film optical characteristics from aforementioned experimental data. The ISR technique and the ISR methods are parts of a whole, which we call simply as 'ISR'.

5.2 Motivation for Development and Exploitation of Imaging Spectroscopic Reflectometry

The aim of any manufacturer of thin films for optical applications is to produce ideal thin films fulfilling specific requirements in their optical properties. Unfortunately, thin films produced under real conditions often exhibit various defects influencing those properties. Ignoring the existence of these defects can lead to significantly distorted or even incorrect values of the optical parameters of these films. This issue is addressed in Chap. 10.

One of the defects mentioned above is the area non-uniformity in the optical properties of a thin film. From the point of view of thin film optics we use the term non-uniformity of thin films, if their optical properties, and therefore, their optical parameters (thickness and optical constants), vary along the area of the films. The most frequent type of this defect, which we can encounter in practice, is the non-uniformity in thin film thickness. Even when the thin film is non-uniform only in thickness, well established (non-imaging) optical techniques, such as conventional ellipsometric and conventional spectrophotometric techniques [1–3] can fail as long as the thickness non-uniformity is of a general type.

This is caused by the fact that the diameter of the illuminating light beam in commercial spectrophotometers and ellipsometers used in optical analysis of thin films is relatively large (usually in the order of mm^2 up to tens of mm^2 depending on the angle of light beam incidence). Consequently, local film thickness variations within an illuminated spot on the surface of the film lead to averaging in the parameters of the film. On the other hand, the measurement of optical properties of thin films using conventional techniques is a local measurement. Therefore, the general non-uniformity in the film thickness cannot be assessed in this way. For this purpose, it

is necessary to scan the studied area of the film, which is time consuming. Another case, in which it is difficult to expect the correct result using a conventional technique, is the characterization of coating of objects with lateral dimensions smaller than the diameter of the illuminating beam. In the field of spectrophotometry several authors [4–8] solved the problem of thin film thickness non-uniformity with the aim to obtain more correct values of film optical parameters from output experimental data provided by conventional spectrophotometers. They assumed that the film non-uniformity in thickness was of a special shape, namely the shape of a wedge. They also assumed that the sample is illuminated by the light beam of a rectangular cross section two sides of which are oriented parallel with the thickness gradient. Unfortunately, the formulae used by them are not applicable in the case of general thickness non-uniformity.

In [9] the reflectance of thin films which are non-uniform in thickness was expressed by means of an integral over the distribution density of the film thickness. This approach to solving the problem of film non-uniformity in thickness is the most general yet. But also this approach does not provide a distribution (map) of the thin film local thickness.

This map can be acquired by scanning an interesting region of the investigated film by means of an illuminating light beam of a reduced diameter (requested spatial resolution of the map is given by a size of the illuminating spot on the film surface). A studied sample is illuminated by a white light beam, the reflected light is gathered from a small sample area by a fiber and then analyzed by an optical spectrum analyzer [10–13]. The scanning is performed either by a 2D movement of a sample holder relative to the immobile fiber or a 2D movement of the fiber relative to the immobile sample. The technique is very time consuming in the case when the investigated film region is large and/or the requested spatial resolution of the measurement is high. It is the significant drawback of the technique.

Several works also took into account the influence of the thin film thickness non-uniformity during evaluation of measurements of thin film optical parameters by means of conventional ellipsometers [14–16].

Again, the approaches presented there do not provide a map of local thin film thickness. It is, therefore, needed to extend the conventional spectrophotometry and ellipsometry to their imaging versions which add a spatial resolution on a sample to the conventional techniques without a necessity of scanning the sample, and thus open up new ways for characterization the optical properties of thin films that vary along the surface of these films. Such imaging techniques are developed particularly in the last decade.

The often utilized technique in the aforementioned problem has been the imaging ellipsometry. We do not deal with this technique in this book, but the relevant information concerning it can be found elsewhere, e.g. [17–25].

We only mention that this technique has certain drawbacks which cause the fact that imaging ellipsometry to have about the same sensitivity as conventional, i.e. non-imaging ellipsometry technique, but lower trueness of results (when data are not repaired). The imaging ellipsometers utilize an imaging system which creates an image of the studied sample mostly on a chip of a CCD camera. That imaging

system is mostly constructed as a microscopic one. This brings a substantial benefit of the spatial resolution on a studied sample, but also leads to certain shortcomings of this imaging technique. The reason of them is that parameters of imaging are not ideal: the angle of incidence is varying in a range given by the numerical aperture of an imaging lens; the numerical aperture must be high to achieve a sufficient spatial resolution; the measurement is averaged over a range of angles circumscribed by this aperture (this problem can be eliminated by a certain correction, which is however not simple); as a result of the possible oblique incidence of the illuminating light beam a sample image is deformed and it is also necessary during the data pre-processing to carry out fusion of images caused by insufficient depth of field of view of the imaging system; the material from which the elements of the imaging system are made defines the spectral range that can be used.

Furthermore, the upgrading the conventional techniques to their imaging versions also increases complexity of the corresponding measurement systems, and, consequently, their price. It is, therefore, desirable to find such an imaging technique that overcomes some of these shortcomings. Such a technique is the non-microscopic imaging spectroscopic reflectometry at normal incidence of light, which utilizes the image of the whole sample. In the following paragraphs we will focus on this technique and we will refer to it as the ISR technique.

Therefore, we will deal neither with the scanning reflectometry techniques [10, 12, 13, 26, 27] nor the microscopic imaging reflectometry [28].

The ISR technique is being developed since the end of 1990s. It has been used and its applicability has been confirmed in many cases [11, 29–41]. It was proven that the ISR technique is a powerful tool for optical characterization of thin films non-uniform in thickness.

5.3 Brief Specification of Non-microscopic Imaging Spectroscopic Reflectometry at Normal Incidence of Light

ISR is specifically intended for characterization of the optical properties of non-uniform thin films. Of course, ISR can also be used to inspect the thin film uniformity. The most general aim of ISR is to obtain maps of local parameters describing the area optical non-uniformity of thin films. However, the most common practical application of ISR is a precise mapping of the thin film thickness and determination of spectral dependence of the optical constants of the film. Regarding its wider aims, ISR can also determine the parameters of the dispersion model used, such as the band gap of a thin film material, the maximum energy limit of the relevant electron transitions, or a parameter proportional to the concentration of electrons participating in the relevant transitions. In some cases, it also can provide maps of the RMS parameter of the upper film boundary roughness.

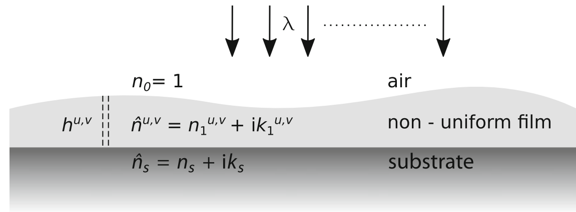

Fig. 5.1 An example of a sample studied by means of ISR

The general situation for a non-uniform thin film is shown in Fig. 5.1. The non-uniform weakly absorbing thin film with thickness and optical constants varying along the area of the film is deposited on an absorbing substrate. A collimated monochromatic light beam impinges perpendicularly on the film from the air. The selected wavelength λ of the beam can vary in a sufficiently wide spectral interval. The response of the whole system on the incident light is given by the local thickness $h^{u,v}$ and the local refractive index $\hat{n}_1^{u,v} = n_1^{u,v} + \mathrm{i}k_1^{u,v}$ of the film ($n_1^{u,v}$ is the real local refractive index, $k_1^{u,v}$ is the local extinction coefficient) and the refractive index of the substrate $\hat{n}_s^{u,v} = n_s^{u,v} + \mathrm{i}k_s^{u,v}$ (we will assume that the absorption of the substrate is so high and/or the substrate is so thick that its lower boundary does not influence the result). The word 'local' means that these local optical parameters of the film characterize the optical properties of the film in a small part of its area and may differ from optical parameters in other areas. These areas form a continuous matrix covering the whole area of the studied film and are labeled with indices u and v. The measured quantity is the local reflectance of the film in a wide spectral range (NUV, VIS and NIR). In the following text, electromagnetic radiation from this interval will simply be called light. From the perspective of optics, thin films are defined as films in which light is undergoing interference. Since we are dealing with such films, the local reflectance is given by the interference of the light between the film boundaries. This simultaneously implies that the ISR technique can be only applied to non-absorbing or weakly absorbing thin films. When a collimated beam of monochromatic light illuminates a thin film perpendicularly, the interference fringes viewed with an imaging system focused on the film are fringes of equal thickness and they are localized within the film [42].

All instruments applied for the ISR technique utilize an imaging system creating an image of the studied sample which is most often recorded by a CCD camera. This imaging system must be focused on the studied film. It is just the imaging process that assigns each $(u, v)^{\mathrm{th}}$ pixel of the CCD camera to the corresponding $(u, v)^{\mathrm{th}}$ small area of the sample surface. The size of these areas should be small enough so that it is possible to consider that the film is uniform within each of these areas.[1] Then the local reflectance of the small $(u, v)^{\mathrm{th}}$ area of the system in Fig. 5.1 corresponding to the $(u, v)^{\mathrm{th}}$ pixel of the CCD camera is given by the following expression:

[1]When the gradient of thickness non-uniformity is so high (e.g. edges of thin films) that the film cannot be considered uniform within those areas, it is possible to perform correction leading to the correct results.

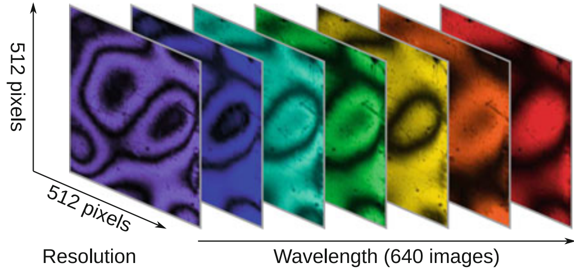

Fig. 5.2 The ensemble of monochromatic images of the studied thin film. This ensemble allows to obtain the map of spectral dependence of the film local reflectance

$$R^{u,v} = \frac{I_r^{u,v}}{I_o^{u,v}} = \left|\hat{r}^{u,v}\right|^2 . \tag{5.1}$$

In the equation above, $I_r^{u,v}$ is the intensity of light reflected by the $(u, v)^{\text{th}}$ area of the film, $I_o^{u,v}$ is the intensity of light incident on the $(u, v)^{\text{th}}$ area of the film and $\hat{r}^{u,v}$ is the local reflection coefficient. This coefficient at normal incidence is expressed as follows:

$$\hat{r}^{u,v} = \frac{\hat{r}_1^{u,v} + \hat{r}_2^{u,v} \exp\left(\mathrm{i}\hat{X}^{u,v}\right)}{1 + \hat{r}_1^{u,v}\hat{r}_2^{u,v} \exp\left(\mathrm{i}\hat{X}^{u,v}\right)},$$

where $\hat{r}_1^{u,v}$ and $\hat{r}_2^{u,v}$ are local Fresnel reflection coefficients on the upper and lower boundary, respectively. The symbol $\hat{X}^{u,v}$ denotes the local phase-shift angle.

$$\hat{r}_1^{u,v} = \frac{n_0 - \hat{n}_1^{u,v}}{n_0 + \hat{n}_1^{u,v}},\ \hat{r}_2^{u,v} = \frac{\hat{n}_1^{u,v} - \hat{n}_s}{\hat{n}_1^{u,v} + \hat{n}_s},\ \hat{X}^{u,v} = \frac{4\pi}{\lambda}\hat{n}_1^{u,v} h^{u,v}.$$

The ability to measure the local reflectance $R^{u,v}$ in each $(u, v)^{\text{th}}$ area of the film brings a spatial resolution compared with the conventional non-imaging reflectometry, without the need for scanning the sample. Changing the wavelength of incident light between the acquiring the successive monochromatic images we can obtain a relatively large ensemble of these images of the film, and in this manner also the map of spectral dependence of local reflectance (see Fig. 5.2).

5.4 Experimental Set Up of ISR Technique

The experimental set up of the ISR technique is simple. Its principal scheme is shown in Fig. 5.3.

A white light source illuminates the input of a monochromator, the monochromatic light beam with a computer-controlled wavelength emerging from the output of the monochromator is split by a beamsplitter. A part of this beam illuminates the studied sample perpendicularly and, after being reflected from the sample, it goes back through the imaging system which creates an image of the sample on the chip of a CCD camera.

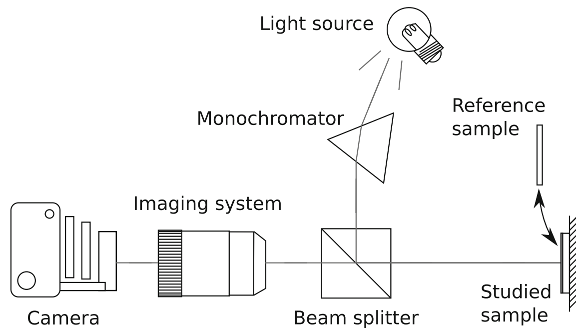

Fig. 5.3 Basic scheme of ISR technique

The normal incidence of a collimated monochromatic light beam on a studied sample brings some benefits. Specifically, we get information from the whole sample surface at once (i.e. without scanning the surface), the interference fringes carrying the necessary information are exactly imaged by means of the imaging system on the CCD camera chip and formulae used for evaluation of required optical parameters are simpler. The disadvantage is that a beamsplitter must be used. The imaging system defines the applicable spectral range. It is better to base this system on reflection optics which works well also in the UV spectral region where the optical properties of thin films are manifested more prominently. The CCD camera must have a good spectral sensitivity within the spectral range, in which the sample is studied. Together with the imaging system, it defines the spatial resolution on a sample. The ISR technique is designed as a relative technique, i.e. the measurement of the studied sample is compared with the measurement of a reference (known) sample under the same conditions. In this way, a possible non-uniformity in the sample illumination is eliminated. Of course, it is necessary to ensure the identical position of the studied and the reference samples. This can be done by means of an appropriate sample holder.

5.5 Imaging Spectroscopic Reflectometers

The concrete implementation of the basic scheme of the ISR technique can be demonstrated by two examples verified in practice.

5.5.1 Imaging Spectroscopic Reflectometer with Wide Spectral Range

The spectral range in which the local reflectance of the studied film is measured must be wide enough, in order to get the information needed for reliable evaluation of the

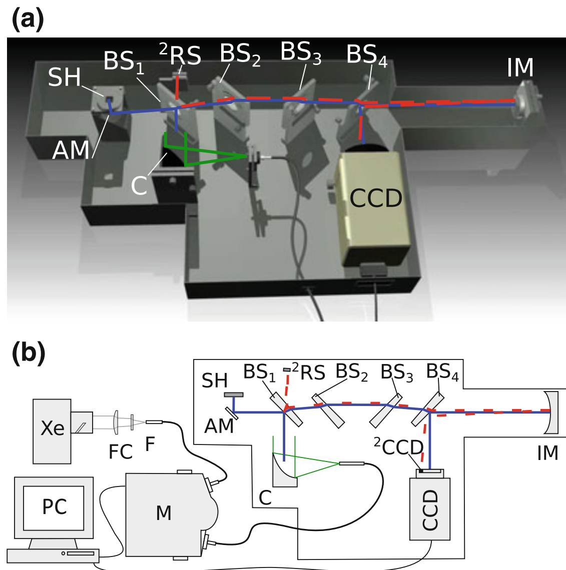

Fig. 5.4 **a** Computer-rendered 3D view of ISRWS (external parts of the whole set up of ISRWS, i.e. the xenon lamp, the monochromator and the control computer are not presented). **b** The three parts of ISRWS experimental set up: The first, illuminating part is a XeUV arc lamp Xe, which is connected to the second part (a monochromator M) by a fiber, a fiber coupler FC and a filter F. The third part (the measuring system) consists of a collimator C, a set of silica wedges BS_{1-4}, an auxiliary mirror AM, a sample holder SH, an imaging mirror IM and a CCD camera CCD. The reference channel of the measuring system consists of a secondary reference channel sample ^{2}RS and a small part of the CCD chip – ^{2}CCD. Everything is controlled by a personal computer – PC

optical parameters. In this context, using imaging systems with refractive optical elements brings issues caused by the dispersion of light in these elements. Furthermore, refractive optical elements manufactured from common optical materials do not work in the UV spectral region in which the optical properties of thin films manifest themselves more prominently. These issues can be effectively resolved by using an imaging system with reflective optical elements. Then, only dispersion of light in a beamsplitter must be tackled. An example of a non-microscopic spectroscopic imaging reflectometer with wide spectral range (ISRWS) which uses such an approach is shown in Fig. 5.4a (computer-rendered 3D view), its scheme is in Fig. 5.4b.

The complete ISRWS system is divided into three distinctive parts connected using optical cables. Although the use of optical cables reduces the overall light throughput on the other hand it allows higher flexibility of the system set up. The three parts of the ISRWS system are: A light source (a UV capable xenon arc lamp Xe), a monochromator M (a commercially available computer controlled Czerny-Turner type monochromator) and an original measuring system itself. The measuring system

consists of a collimator (a single off-axis parabolic mirror C), a sample holder SH, a set of fused silica wedges BS_1–BS_4 (some used also as beamsplitters), a spherical imaging mirror IM and a UV-VIS CCD camera. The monochromator with the xenon lamp connected serves as a source of monochromatic light for the measuring system and thanks to the use of fiber optics it can be easily used as a source for other devices as well. In the measuring system the divergent monochromatic light beam is collimated by the collimator and then it is directed at the measured sample using the first fused silica wedge (functioning as a beamsplitter in a way described in Sect. 5.4). In this way a normal incidence of light on the sample can be achieved. Light reflected from the measured sample is then directed through all four silica wedges. The first one serves as the aforementioned beamsplitter, while the others are used to eliminate secondary reflections from the main light path. The fourth wedge is also used as a beamsplitter to allow in-axis imaging by the imaging mirror located behind all the silica wedges. The image created by the optical system is then recorded by the chip of the CCD camera. Light, which initially passes through the BS_1 is not used for imaging of the measured sample. In fact, it contributes to the losses of light intensity. But it can be exploited in a reference channel to measure and subsequently eliminate possible fluctuations of the source light intensity. This is realized using a secondary reference sample which is imaged on the CCD camera chip at the same time as the measured sample (there is a specifically reserved part of the CCD chip for this purpose). The principle of this idea is that the secondary reference sample is never replaced or moved between a series of sample measurements so it is possible to observe intensity changes of the source light. The ISRWS is capable of measuring samples of maximum size about 20 mm × 20 mm while maintaining spatial resolution of 9 lp/mm.

The spectral range spans from 270 to 1000 nm (1.2–4.6 eV). The duration of a measurement of a single sample measurement is typically 30 min (not including the measurement of a reference sample and the background, which need not to be measured every time).

5.5.2 Imaging Spectroscopic Reflectometer with Enhanced Spatial Resolution

An example of a very simple instrument allowing an implementation of the ISR technique is the imaging spectroscopic reflectometer with enhanced spatial resolution on a sample (ISRER).

The ISRER was designed as a low cost, simple instrument for optical characterization of thin films with high gradients of non-uniformity. Its computer-rendered 3D view is shown in Fig. 5.5a and its basic scheme is in Fig. 5.5b.

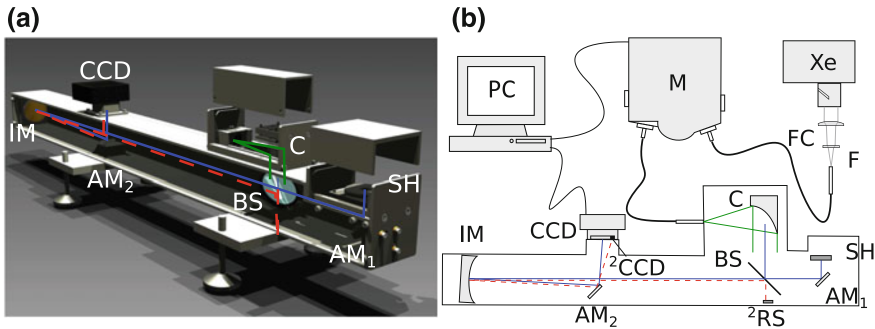

Fig. 5.5 **a** Computer-rendered 3D view of the ISRER (external parts of the whole set up of the ISRER, i.e. a xenon lamp, a monochromator and a control computer are not presented). **b** Basic scheme of the complete ISRER. A xenon UV arc lamp Xe is connected to a monochromator M by a fiber, a fiber coupler FC and a filter F. Measuring system itself consists of a collimator C, a membrane (pellicle) beamsplitter PB, two auxiliary mirrors AM_{1-2}, a sample holder SH, an imaging mirror IM and a CCD camera CCD. The reference channel is realized by a secondary reference sample ^{2}RS and a small part of the CCD chip (^{2}CCD). The whole system is controlled by a personal computer PC

A monochromatic light source (the lamp and the monochromator) for the ISRER is the same as used in the ISRWS, only the measuring part of the ISRER is different. The main difference is the usage of a membrane (pellicle) beamsplitter instead of the four silica wedges. The advantage of the pellicle beamsplitter is the low thickness of the membrane which in a sense eliminates the influence of the secondary reflection (the secondary reflection is so close to the primary reflection that they cannot be distinguished and therefore does not degrade the captured image). Since there is no additional beamsplitter used, the imaging is realized as slightly off-axis imaging (when using an auxiliary mirror AM_2 to reduce the off-axis angle) which brings the benefit that the light intensity hitting the CCD chip does not decrease significantly (use of even an ideal beamsplitter results in 75% loss of intensity). Although the spatial resolution of the ISRER is significantly higher than of the ISRWS, it is still low enough not to be affected by the off-axis imaging setup. The reference channel is realized in a similar way as in the ISRWS by the use of a reference channel sample. The size limit of the measured sample for the ISRER is about 20 mm × 15 mm (a bit less than ISRWS) but the measurement can be done with spatial resolution of 16 µm × 16 µm on a sample. The spectral range from which the wavelengths can be selected spans from 400 to 1000 nm.

The maximum value of thickness gradients is 12.5 µm/mm. The possibilities of the ISRER in the case of thin films with high gradients in thickness are demonstrated in Figs. 5.6 and 5.7.

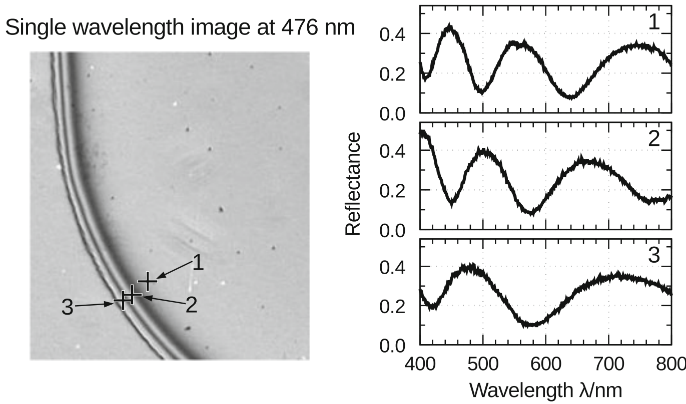

Fig. 5.6 Edge of a HfO_2 film – a map of local reflectance for $\lambda = 400\,\text{nm}$ (raw data multiplied with reflectance of the reference sample) and spectral dependencies of reflectance for three selected CCD pixels

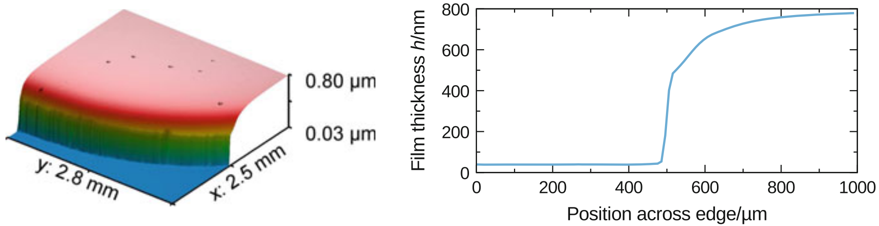

Fig. 5.7 3D representation of the film edge from Fig. 5.6 and profile of the film edge perpendicular to this edge

5.6 Data Acquisition

Both aforementioned imaging spectroscopic reflectometers measure spectral dependencies of local reflectance of a sample studied. From the ensemble of these data the values of spectral dependencies of local relative reflectance $R_r^{u,v}(\lambda_k)$ of the sample are obtained. These values for a given wavelength λ_k are arranged in a matrix. The $(u, v)^{\text{th}}$ element of this matrix corresponds to the $(u, v)^{\text{th}}$ pixel of the CCD camera recording the image of the studied sample at the wavelength λ_k. It means that this matrix element $R_r^{u,v}(\lambda_k)$ corresponds to the $(u, v)^{\text{th}}$ small area on the sample surface which is imagined on the above mentioned $(u, v)^{\text{th}}$ CCD pixel. Indices of these individual small areas imaged on corresponding pixels of the CCD camera take values $u = 1...U$; $v = 1...V$. U and V are the numbers of pixels of the CCD chip in horizontal and vertical directions and are given by the CCD camera resolution. The matrix as a whole corresponds to the imaged area of the sample. When measuring, the wavelengths λ_k are suitably selected (accordingly to the presumed spectral reflectance of the studied sample) from the usable spectral range of the given imaging spectroscopic reflectometer (ISRM) with a chosen sampling step. In this way an ensemble of matri-

ces is obtained from the set of sample images (see Fig. 5.2). Vectors formed from matrix elements with the same indices u and v represent sought spectral dependencies of the sample local relative reflectance. This 'map' of spectral dependencies of the sample local relative reflectance is used for the determination of optical parameters of a studied thin film. In order to eliminate the temporal fluctuations in the light source intensity, both reflectometers were designed as two-channel instruments. Retrieving the experimental data of a sample using both the reflectometers is a three-step procedure consisting of the measurement of a reference sample (measured at the time t_1), the measurement of the sample to be studied (measured at the time t_2), and the measurement of the background signal (measured at the time t_3). The background signal can be expressed as follows:

$$S^{u,v}(\lambda_k, t_3) = D_f^{u,v}(\lambda_k, t_3) + b^{u,v} I_o(\lambda_k, t_3),$$

where $I_o(\lambda_k, t_3)$ is the intensity of the monochromator output at the wavelength λ_k and at the time t_3, $b^{u,v}$ is the constant of proportionality, $b^{u,v} I_o(\lambda, t_3)$ is the response of the CCD camera to the light scattered inside the reflectometer, $D_f^{u,v}(\lambda_k, t_3)$ is the dark frame (it contains the whole signal which is generated by the CCD chip without being exposed to any light) obtained at the closed CCD camera shutter at the exposure time and the chip temperature identical to the actual measurement of the sample. This dark frame is acquired immediately after obtaining the relevant signal and it is subtracted. Therefore, the dark frame is not mentioned further in the text. After eliminating the dark frame, the whole three-step procedure of the experimental signal processing may be concisely expressed as follows: The signal already without the $D_f^{u,v}$ obtained from a single pixel with coordinates u and v can be written as

$$S_{J,i}^{u,v}(\lambda_k, t_i) = I_o(\lambda_k, t_i)[\eta^{u,v}(\lambda_k) R_i^{u,v}(\lambda_k) + b^{u,v}], \tag{5.2}$$

where index J can take two values: value m, which stands for 'measuring channel' and value s for 'reference channel', index i can be of value 1, 2 or 3 according to the kind of the measurement (1 is for the measurement of the reference sample, 2 is for the measurement the studied sample and 3 is for the measurement of the background i.e. without the sample).

$I_o(\lambda_k, t_i)$ is again the intensity of light on the monochromator output at the wavelength λ_k and at the time t_i, $\eta^{u,v}(\lambda_k)$ describes all the influences of the apparatus, e.g., effects of possible imperfections in optical elements and/or bad pixels of the camera, but also the signal amplification or camera bias, noise etc. $R_i^{u,v}(\lambda_k)$ is the absolute local reflectance of the current sample given by the index. Since the reflectance is equal to 0 for index $i = 3$ (blank measurement without any sample), the first addend in the formula (5.2) is also equal to 0 and only the background $I_o(\lambda_k, t_i) b^{u,v}(\lambda_k, t_3)$ remains. The following formula (5.3) ensures that any temporal instability of the light source of the ISRM is eliminated (i.e. it removes the time dependence of the $I_o(\lambda_k, t)$). It also removes the influence of the background and of any non-uniformity in the illumination of samples:

$$R_r^{u,v}(\lambda_k) = \frac{\frac{S_{m,2}^{u,v}(\lambda_k,t_2)}{S_{s,2}(\lambda_k,t_2)} - \frac{S_{m,3}^{u,v}(\lambda_k,t_3)}{S_{s,3}(\lambda_k,t_3)}}{\frac{S_{m,1}^{u,v}(\lambda_k,t_1)}{S_{s,1}(\lambda_k,t_1)} - \frac{S_{m,3}^{u,v}(\lambda_k,t_3)}{S_{s,3}(\lambda_k,t_3)}} = \frac{R_2^{u,v}(\lambda_k)}{R_1^{u,v}(\lambda_k)}. \tag{5.3}$$

This is the spectral dependence of the local relative reflectance of the studied sample in the spectral range chosen in the measurement. In this way we acquire a map of such local reflectance spectral dependencies (see Fig. 5.6). The duration of a single sample measurement is typically 30 min (without the measurement of a reference sample and the background, which need not to be measured every time).

5.7 Key Features of Imaging Spectroscopic Reflectometry

At the end of our treatise on ISR technique, we will summarize the main features of this technique as follows:

- A CCD camera records *monochromatic images* of a *relatively large area* of a studied film, which are *created by an imaging system within wide span of wavelengths*.
- A small region of the film surface is assigned to a one pixel of the CCD camera by *the process of imaging*.
- These areas are so small that the film can be considered *uniform within individual areas*.
- The ISR technique is *a relative technique*. The spectral dependence of the local reflectance of the studied sample is measured against the spectral dependence of the local reflectance of a reference sample (mostly a silicon single crystal wafer).
- The output experimental data of the ISR technique are the *maps of spectral dependence of the thin film local relative reflectance*.
- *Normal incidence* of the collimated beam of light illuminating the sample *eliminates the necessity of scanning and also image fusion* during postprocessing the output experimental data.

5.8 Methods of Imaging Spectroscopic Reflectometry

As mentioned in the introduction, we consider an ISR method as a way of experimental data processing, through which we determine interesting optical parameters of a thin film. These methods are an integral part of the determination of the optical parameters of thin films. The experimental data obtained by means of the ISR technique are the maps of spectral dependence of the local thin film reflectance. This fact defines the limit of the information content of these data. The different methods of the data processing give a different level of information we can get within this limit. Their specific feature is that they must handle enormous amounts of experimental data (assuming an image 500 $\times$ 500 pixels large with a 500-point spectrum in each pixel the number of data points is 1.25×10^8) and also to determine a huge amount

of the thin film parameters (the number of parameters searched can be estimated to be about 2.5×10^5). This means that it is not possible to simply use the standard form of Levenberg–Marquardt non-linear least-squares fitting algorithm for the determination of thin film parameters but it is necessary to develop original algorithms for this purpose. On the other hand, this enormous amount of experimental data eliminates random errors of the thin film parameters. Therefore, the determined values of the parameters have only systematic errors. The ISR methods are discussed in detail in Chap. 6, where their mathematical formulation is presented.

It is also important to stress another significant feature of the ISR methods. Most of thin film parameters that are sought are practically always mutually correlated. Then, it is impossible to determine them unambiguously. To overcome this problem, the multi-sample method must be applied to improve the stability of least-squares data fitting (e.g. [43]). The ISR technique, performing independent measurements in individual CCD pixels, inherently provides data for a multi-sample method. Now we will focus on the classification of these methods and, simultaneously, we will present selected demonstrations of individual ISR methods in order to illustrate their possibilities. We will classify the ISR methods from the viewpoint of the way in which the information provided by CCD pixels is used. It should be emphasized that this classification can only be schematically. The reason is that the use of the ISR method depends not only on the task which we solve, but also on our decision what method we want to use. For example, when aiming to determine the local thickness of a thin film with a known spectral dependence of the optical constants, the relevant ISR method can be used as the stand-alone method. But if we aim to characterize a thin film which differs very much from an ideal one (for example a film exhibiting more defects) and/or with a complicated form of spectral dependencies of optical constants, we probably would have to use the method in combination with other methods of film characterization (i.e. conventional ellipsometric or spectrophotometric) and the ISR method should be used as a complementary method. However, sometimes we can also use the relevant ISR method for the latter film as the stand-alone method. The schematic classification is presented in Fig. 5.8.

We will mark an ISR method as the single-pixel method when the spectra of local reflectance measured by individual CCD camera pixels are processed separately. When those spectra are processed simultaneously the method is called the multi-

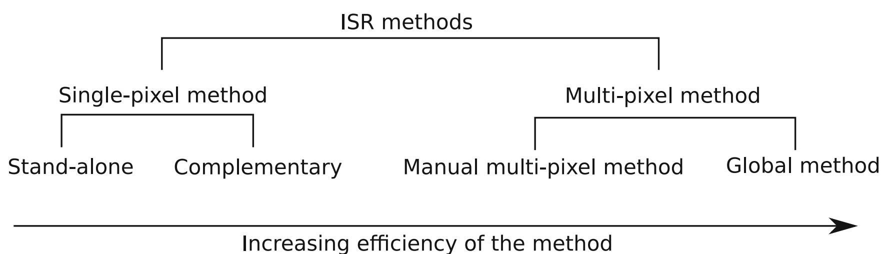

Fig. 5.8 Scheme of ISR methods classification

pixel method. We will start our demonstration of the individual methods with the case where the ISR method can be applied as the stand-alone single-pixel method.

5.8.1 Single-Pixel ISR Method as the Stand-Alone Method

The single-pixel ISR method can be applied as the stand-alone method for optical characterization of a non-uniform thin film, as long as it is possible to suppose that the film does not exhibit another structural defect than non-uniformity in thickness, the film is uniform in optical constants and the spectral dependence of optical constants of this film is relatively simple (or even known) within the interesting spectral range.

Then the number of parameters appearing in the dispersion model describing the spectral dependence of those optical constants is small as opposed to the case when the spectral dependence of the optical constants is complex. In that case all these dispersion parameters and local thickness can be determined independently by a fitting procedure separately in each pixel.

The aforementioned case can be demonstrated using carbon-nitride films, which were deposited onto silicon single crystal wafers by a dielectric barrier discharge with CH_4/N_2 gas mixture (details of the technological procedure used to prepare the films are given in [44]). When treating the experimental data, the dispersion model based on parametrization of the joint density of electronic states (PJDOS) corresponding to amorphous materials [45] was used. It was assumed that the films contain no defects other than the thickness non-uniformity.

It was found that those films can be considered uniform in the optical constants (the determined values of dispersion model parameters were practically the same in all film areas which corresponded to the individual pixels of a CCD camera). Spectral dependence of these optical constants determined from the parameters of the above-mentioned corresponding dispersion model are presented in Fig. 5.9a for a sample selected from a measured file of those films. The 3D map of the local thickness of this carbon-nitride film is shown in Fig. 5.9b.

The maps of the spectral dependence of the local relative reflectance got from ISR measurements exhibit noise. This implies that the maps of the local thickness and the values of the film optical constants determined from individual CCD pixel inevitably exhibit noise as well. The reflectance values $R^{u,v}$ were measured with the statistical relative error about 1% (corresponding to the standard deviation). Using a standard error analysis, it was found that the values of the local thicknesses in the area distributions were determined with the statistical relative error of 1–2% (corresponding to the standard deviation). The same conclusion concerning the accuracy was also found for the optical constants.

The single-pixel ISR method is simple. That is its main advantage. Unfortunately, this method cannot be applied when the characterized non-uniform thin films exhibit a complicated course of spectral dependence of the optical constants requiring the usage of a dispersion model with a larger number of parameters and/or exhibit further defects than non-uniformity in thickness (such as the roughness of boundaries,

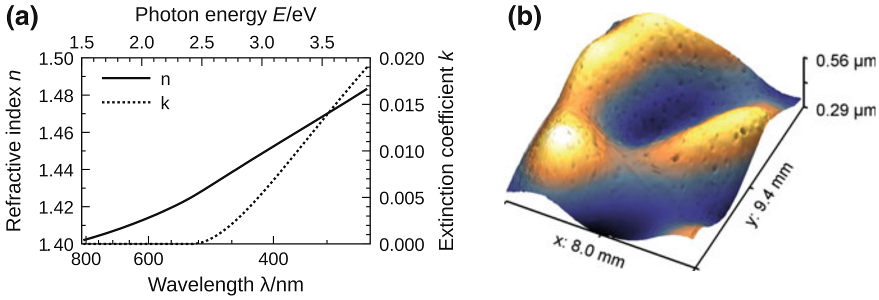

Fig. 5.9 **a** Spectral dependence of the refractive index n and the extinction coefficient k of the selected non-uniform carbon-nitride film. **b** 3D map of the local thickness of this carbon-nitride film determined using the ISR method

very thin overlayers on the upper boundary or very thin transition layers between the substrate and the film). Then it is necessary to complete this ISR method with other methods such as conventional (non-imaging) spectroscopic ellipsometry and conventional (non-imaging) spectrophotometry. The detailed description of this method application to the presented case can be seen in [36]. Other applications can be found in [32, 33].

5.8.2 *Single-Pixel ISR Method as the Complementary Method*

In this case, the single-pixel ISR method is applied in combination with other optical methods (e.g. ellipsometric and/or spectrophotometric). It plays a role of a complementary method to these other methods, i.e. the method which allows us to obtain values of the local thin film parameters by which it is possible to characterize a non-uniformity of the film along its surface (e.g. local thickness or local roughness), while the film optical constants that can be supposed to remain unchanging along the entire surface of the film are found by means of the above mentioned other methods. As the demonstration example of the case where the single-pixel ISR method is used as the complementary method in combination with other optical methods, we will present the optical characterization of a selected sample of considerably non-uniform $SiO_xC_yH_z$ thin films deposited using plasma enhanced chemical vapor deposition onto a silicon single-crystal wafer (the detailed preparation of the film see [11]). Three optical techniques, i.e. conventional variable-angle spectroscopic ellipsometry (VASE), mapping spectroscopic ellipsometry with microspot (μSE), and ISR were used for the film characterization. Both ellipsometric techniques were used to determine spectral dependence of the optical constants of the studied film. Moreover, μSE was used to evaluate uniformity of the film in its optical constants and the type of the film thickness non-uniformity. For this purpose μSE measurement was car-

ried out in 99 sample positions that formed a regular 11 × 9 grid with 1 mm spacing. Experimental data acquired by the ISR technique were used for the determination of the map of the film local thickness. The experimental data obtained by means of ellipsometric techniques were processed by the Levenberg–Marquardt algorithm using the following structural model of the film: The film is without defects except the thickness non-uniformity, i.e. the material of the film is optically isotropic, it is homogeneous in the direction perpendicular to the sample plane, the film boundaries are sharp and smooth, and the thickness non-uniformity is of the wedge type. Moreover, it is assumed that the film optical constants do not vary within the region corresponding to the microspot used in μSE (the circle 250 μm in diameter for normal incidence). In the case of ISR, the film is assumed as uniform within the region corresponding to a single pixel of the CCD camera. The film complex refractive index was modeled using an expression for SiO_2–like materials based on PJDOS [45]. The single pixel ISR method was utilized as the complementary method to conventional VASE and μSE. Spectral dependencies of the film optical constants were found by fitting VASE data. Subsequently, reflectance spectra in individual pixels obtained by ISR were fitted, utilizing the optical constants obtained by ellipsometry and assuming they were correct. The results obtained are presented in Fig. 5.10.

Since it is not feasible to display the error bars for all the 99 μSE curves in Fig. 5.10, the errors will be summarized numerically. The average three standard deviations error estimate for the refractive index n was about 0.013 in the whole spectral range, whereas for the extinction coefficient k it varied from approximately 0.01 at the UV end of the spectrum to 0.001 at the IR end. It is evident from Fig. 5.10 that the error bars of the conventional VASE and μSE overlap. The results are thus in agreement. No trend was found in the area distribution of refractive index values obtained by means of μSE. Their fluctuations represented random experimental errors and the same can be said about the extinction coefficient. Therefore, no evidence of non-

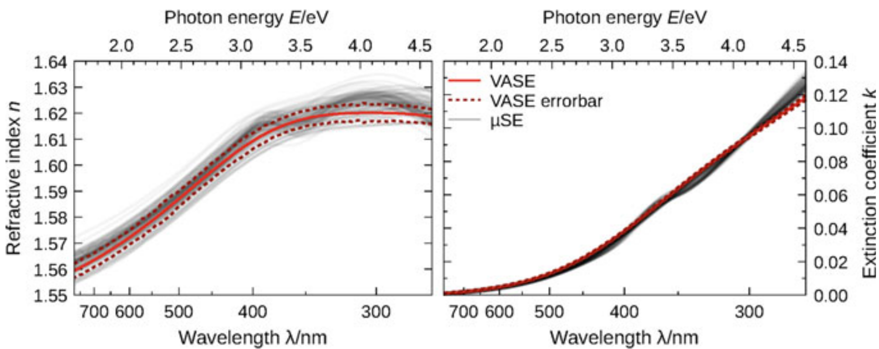

Fig. 5.10 Comparison of spectral dependencies of optical constants, i.e. refractive index and extinction coefficient determined using conventional VASE (solid thick lines), using single-sample μSE in all 99 individual locations (thin shaded lines), and using multi-sample μSE (dotted lines). Error bars corresponding to three standard deviations are plotted for the conventional VASE as dashed lines [11]

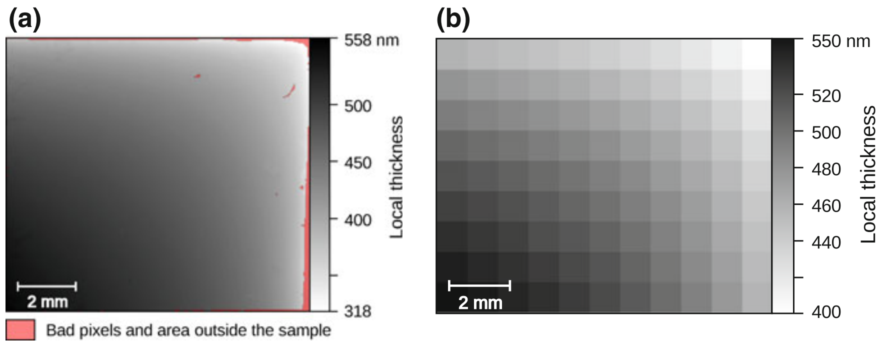

Fig. 5.11 **a** Map of film local thickness obtained by ISR data fitting. Pink regions along the right and top edges correspond to bad pixels and pixels outside of sample. **b** Map of film local thickness determined using μSE [11]

uniformity of optical constants was found within the experimental precision. It is worth pointing out that such conclusion is typical according to our experience. In other words, even if the film is considerably non-uniform in thickness its optical constants can usually be still considered uniform.

Because of the aforementioned consistency of the values of optical constants obtained by conventional VASE and μSE, the spectral dependence of the optical constants determined using conventional VASE was utilized for determining the fine local thickness map by the ISR presented in Fig. 5.11a. The corresponding map found using μSE is shown in Fig. 5.11b.

An exact comparison of the maps of local thickness determined by using ISR and μSE is not possible because it is not possible to ensure exactly the same position of the sample during both the measurements. However, the trend of both the maps allows us to conclude that both the measurements are in agreement. Finally, it can be said that the combination of conventional VASE, μSE and ISR represents a precise tool for optical characterization of thin films non-uniform in thickness. Unfortunately, it is not convenient for routine use because the analysis of the discussed film by means of μSE took approximately five days. Other cases, in which the single-pixel ISR method is applied as the complementary method in combination with other optical methods, are published in [35, 38], where the ISR method is applied in combination with conventional VASE and conventional spectroscopic reflectometry (SR) at near normal incidence. Again, the latter two methods served to determine the spectral dependence of the optical constants and the single-pixel ISR method to determine the fine map of the local thickness of the films exhibiting a thickness non-uniformity only.

In conclusion of this paragraph, it is necessary to make the following note. If the thin film is considerably non-uniform in thickness, it is possible to suspect that the deposition process was not sufficiently uniform and the film material would also be non-uniform along the film, although this material non-uniformity is probably smaller than the thickness non-uniformity. This implies that the film could be non-uniform

in the optical constants as well. Unfortunately, the salient feature of reflectance spectra, interference in the film, depends primarily on the product of film thickness and refractive index, called optical thickness. This makes difficult to distinguish non-uniformities in thickness and optical constants. Therefore, in the case where the conventional methods do not determine optical constants correctly the single pixel ISR method utilized together with those conventional methods leads also to incorrect results. This fact limits the applicability of the results of the single-pixel ISR method in the case under consideration.

5.8.3 Manual Multi-pixel ISR Method

When the single-pixel ISR method processes spectral dependencies of the film local reflectance fitting the dispersion model parameters independently in each pixel, the resulting maps exhibit high noise. On the other hand, it is not possible to simply fit the ISR data in all the pixels together using one set of shared dispersion model parameters. The total number of fitting parameters is huge and they are all correlated. Nevertheless, these two problems can be solved, as we will demonstrate in the case of strongly non-uniform thin films deposited from hexamethyldisiloxane on silicon substrates by a single capillary plasma jet at atmospheric pressure. The detailed description of the preparation of these films can be found in [37]. The manual multi-pixel ISR method has been used as the stand-alone method in that case. The procedure had three steps and each step involved only least-squares fitting problems with reasonable numbers of parameters:

First step: Film thickness is fitted independently in each pixel using the model of an ideal thin film and an initial estimate of film optical constants. In this particular case tabulated optical constants of SiO_2 were used. The thickness maps obtained in this way are not yet correct, but this first step is sufficient to distinguish good and bad pixels in the image of the film. The criterion for it is the agreement between experimental local reflectance spectral dependence and its fit in manually selected pixels representatively covering the region of interest. The pixel selection should respect the requirement to cover the full range of values of the sought parameters. The evaluation of this agreement is done subjectively.

Second step: A set of several (e.g. ten) good pixels was selected manually. The experimental data corresponding to those pixels were fitted simultaneously assuming common optical constants. The large variation in thickness within the selected spectrum set helps reducing the correlation between the thickness and dispersion model parameters and improves stability of the fitting procedure (the multi-sample approach). The PJDOS dispersion model for SiO_2 like materials [45] was used for the films, values of Si substrate values were taken from the literature [46].

Third step: Film thickness is again fitted independently in each pixel, but this time utilizing optical constants found in the second step. The spectral dependence of the film real refractive index is presented in Fig. 5.12. Even though the dispersion model

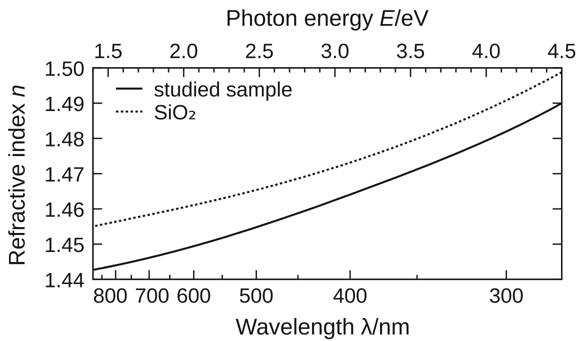

Fig. 5.12 Spectral dependence of the refractive index of the plasma jet thin film compared with the refractive index of thermal SiO_2

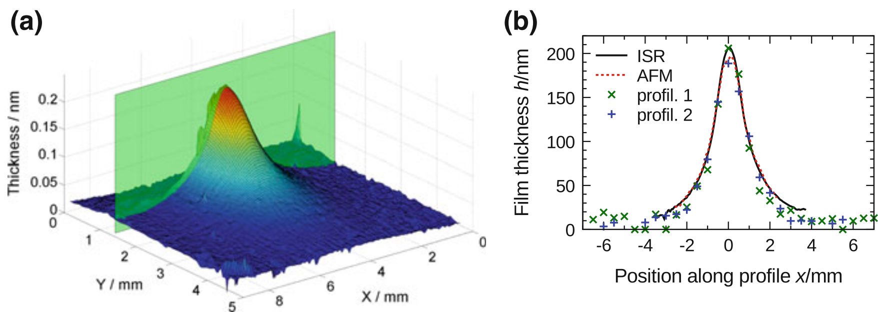

Fig. 5.13 **a** Map of local thickness with selected profiles along the artificial edge of the film. **b** Comparison of thickness profiles along the edge of the film measured by ISR, AFM and the tactile profilometer [37]

permitted absorption, it was found that the film was essentially non-absorbing in the spectral range of the measurement. The extinction coefficient is therefore not shown.

The 3D map of the local thickness of the film obtained as the final result of the procedure described above is presented in Fig. 5.13a. In this figure, the artificial edge created by scratching away a half of the film by means of a scalpel can be seen. The thickness of the film was also measured with a Veeco Dektak profilometer. This measurement was performed with a step of 0.5 mm along the edge (i.e. in the plane in Fig. 5.13a) twice. Finally, the film edge was measured using a Bruker Dimension Icon atomic force microscope in the ScanAsyst mode. Utilizing a motorized table for accurate movement between successive scans, 50 images were acquired and in each the step height was then evaluated.

All measurements were compared using 2D profiles defined by the green plane in Fig. 5.13a. This comparison of the profiles obtained by all three measurement tools is plotted in Fig. 5.13b.

Considering the uncertainty of the individual measuring tools, the agreement of the results obtained can be considered good. Figure 5.13b also shows a strong thickness non-uniformity of the studied thin film. The largest gradient of local thickness in the

smooth part of the film (excluding the edges and debris), determined from inter-pixel thickness differences, was approximately 1.6×10^{-4}. The analysis of experimental errors of the discussed ISR method found that the accuracy of local thickness measurements was approximately 2 nm. The limiting factor was the uncertainty of optical constants of the film as they represented the largest uncertainty source. Finally, we can state that the discussed ISR method was successfully applied as the stand-alone method for determining the optical constants and local thickness map of the film strongly non-uniform in thickness.

5.8.4 Global Method

Although the manual multi-pixel method presented in the previous paragraph works well in practice, it has several shortcomings. Firstly, to do the fitting, it is necessary to manually find a small, yet representative, subset of pixels with a good spectral dependence of local reflectance from the region of interest. It is somewhat unsatisfactory that this choice is subjective and is irreconcilable with automation of data analysis. Moreover, not utilizing entire available data means that the contribution of random noise to parameter uncertainties is larger than necessary. If the analysis utilizes all available data, i.e. reflectance curves from all pixels, random errors can become insignificant compared to systematic errors and thus effectively eliminated.

Therefore, on the assumption of a thin film non-uniform in thickness only, an original experimental data processing procedure has been developed, utilizing the specific structure of the least-squares problem related to the main task of ISR. The basic features of this procedure consist in splitting the free parameters into thicknesses (local parameters, possibly different in each pixel) and dispersion model parameters (shared parameters common for all pixels). Subsequently, both kinds of parameters are fitted by turns, utilizing an unmodified Levenberg–Marquardt algorithm. However, this algorithm is used in such a way that the local thicknesses are corrected during the dispersion model parameters fitting step to preserve the effective optical thickness (product of film thickness and refractive index). This brings a substantial improvement in the procedure convergence and permits the analysis of large imaging reflectometry data sets with reasonable computational resources. The reason for using the condition of preservation of the effective optical thickness is that it is the optical thickness what determines the locations of interference minima and maxima in a reflectance spectrum. The minima and maxima thus move in response to changing optical thickness. When the theoretical reflectance curve already corresponds relatively well to the experimental points, the sum of the squared differences will always increase even if the extrema shift only slightly. The fitting algorithm thus becomes unable to progress further by updating thicknesses and dispersion model parameters separately once the tiniest changes are now permitted. This limitation grows more severe with increasing film thickness since the extrema are spaced more closely for thicker films. The precise analysis of the ISR experimental data processing described just above is presented in [47], where this approach was used for the

Table 5.1 Characteristics of the experimental ISR data sets and fitting parameters for the two thin films

Film	$SiO_xC_yH_z$	CN_x:H
Number of fitted spectra M	70,310	85,469
Points per spectrum K	656	628
Data set size [MiB]	176	205
Free shared parameters D	5	5
Shortest fitting time [s]	540	624

first time. It was applied to the case of two thin films of different amorphous materials deposited on silicon substrates, both exhibiting strong thickness non-uniformity.

The first sample was a hydrogenated carbon-nitride film (CN_x:H) prepared in an atmospheric pressure dielectric barrier discharge from CH_4:N_2 =1:10 gas mixture. The second sample was a $SiO_xC_yH_z$ film deposited in a low pressure radio frequency (13.56 MHz) capacitively coupled discharge from the mixture of tetraethoxysilane and methanol (The details of the deposition procedure can be found in [47]). The same structural and dispersion models were used for both films. The films were considered ideal within a single ISR pixel. The complex refractive index was modeled using an expression for SiO_2-like materials based on PJDOS [45]. Straightforward parallelization on data was applied. It was demonstrated that the strategy of preserving quantities corresponding to effective optical thicknesses in individual pixels resulted in the fastest convergence of the least-squares fit. It was also shown that even though a behavior of the algorithm deteriorates above a film thickness of approximately 600 nm, the result was still acceptable. The sizes of the data and fitting parameter sets are summarized in Table 5.1 for both thin films. The table also includes the time duration of the computation running on a reasonably powerful personal computer (six-core AMD Phenom II processor and 16 GiB of RAM). The computation times listed in Table 5.1 evince that the developed fitting procedure made a global ISR data analysis possible, even with relatively modest computational resources.

The reduction of parameter errors and improved reliability of results following from multi-pixel data fitting may be beneficial in the characterization of samples that could be characterized also by other means. However, the key advancement is that a wider range of samples can now be characterized using ISR as a stand-alone method, without resorting to combination with conventional ellipsometry and spectrophotometry. Because this method exploits the experimental data of all pixels in the image of the film in the way that the shared parameters and local parameters are fitted continuously during the fitting procedure, it can be named as the global method.

To show the real power of this method, an application of the method for characterization of a thin film, which is far from an ideal one, is presented here. A ZnSe film prepared by molecular-beam epitaxy (MBE) on a (100) GaAs single crystal substrate can serve as a good example (for detailed deposition parameters see [40]). Epitaxial ZnSe thin films deposited on GaAs substrates by means of MBE have randomly rough

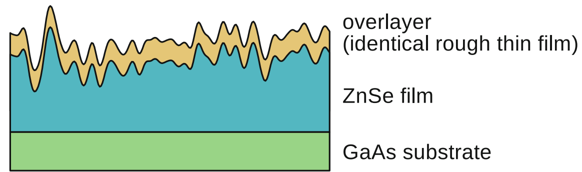

Fig. 5.14 Schematic depiction of the structural model of the film

upper boundaries. This roughness arises from the mosaic (or block) structure of the films [48]. MBE normally produces thin films that are fairly uniform along the substrate plane. However, it is sometimes possible to encounter ZnSe epitaxial thin films whose thickness varies to such extent that they need to be considered non-uniform. Of course, when both imperfections, surface roughness and thickness non-uniformity, occur together, then film characterization is more difficult. The structural model of the film under consideration is shown in Fig. 5.14.

Since the ZnSe thin film with a rough upper boundary was placed in the air, it was covered with a very thin overlayer [49]. This overlayer was modeled as so-called identical rough thin film, i.e. a film with upper and lower boundaries that are exact geometrical copies of each other (see also Fig. 6.4). When lateral correlations play no role, a single number is then sufficient to describe the roughness, the RMS of height irregularities. The substrate–film boundary was assumed to be smooth. Although the film was relatively non-uniform in thickness, within the range of the surface corresponding to a single pixel of a CCD camera, the film was considered uniform in thickness.

The optical constants of the ZnSe film were expressed using a PJDOS model for valence-to-conduction inter-band transitions [50, 51] and fitted. Tabulated values found in earlier studies were used for both the overlayer [49] and the GaAs substrate [52].

Scalar diffraction theory (SDT) was used to model the influence of the upper boundary roughness on reflectance [53]. The expressions resulting from SDT have the form of an infinite series. This series was rewritten into a form suitable for an efficient evaluation by computers. In particular, the computation time was made almost independent on the precision to which the series was evaluated, eliminating the need to make any trade-offs between precision and speed in SDT computations. This is the great advantage in comparison with the Rayleigh–Rice theory (RRT) [53] which has been used for modeling of the upper boundary roughness influence for the optical characterization of the same (discussed above) ZnSe thin film in [38], where the single-pixel ISR method has been used in combination with conventional VASE and SR. The influence of the roughness is described by very complicated formulae within RRT. This is significant in the case of ISR, when large numbers of experimental data must be processed, and would lead to very long data processing times. The fitting algorithm described in this paragraph has led to a satisfactory fit essentially in the whole image of the film. It is illustrated in Fig. 5.15.

Since the optical constants of the ZnSe film were modeled and fitted in the ISR data analysis, it was possible to compare the obtained spectral dependencies with

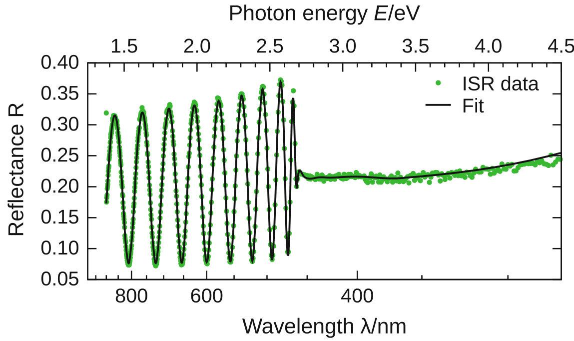

Fig. 5.15 Selected typical ISR spectrum of the ZnSe film on GaAs and its fit by the theoretical model. The spectrum corresponds to a pixel close to the image center [40]

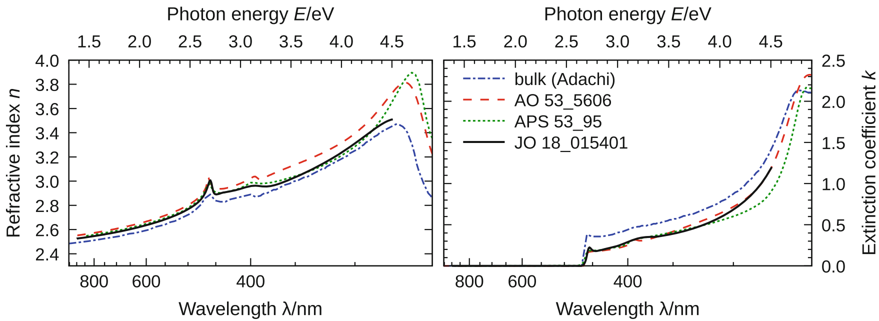

Fig. 5.16 Spectral dependencies of optical constants of the ZnSe film. The curves denoted 'AO 53_5606', 'JO 18_015401', 'APS 53_95' and bulk (Adachi) represent optical constants found for epitaxial ZnSe in [38, 40, 54] and optical constants of bulk ZnSe [55], respectively [40]

those found in other works. This comparison is shown in Fig. 5.16, where also the dependencies for the same film determined in [38] by VASE, for epitaxial ZnSe films studied in [54] and for bulk ZnSe [55] are presented.

The agreement between the results presented in Fig. 5.16 can be considered good. The uniformity of the film in the optical constants was also checked by dividing the ISR data into four quadrants and rerunning the fitting procedure individually for each quadrant. Parameters controlling the overall shape of the complex refractive index curve were fitted, but parameters determining the locations of fine structures in the spectral dependencies were fixed in values obtained from the whole data.

Considering typical experimental errors of the method, all four obtained spectral dependencies were indistinguishable. The initial assumption that the film material could be considered uniform was thus justified.

Maps of local film thickness h, the RMS surface roughness and thickness of the overlayer are presented in Fig. 5.17. The artefacts which can be seen in both the maps of the RMS roughness and overlayer thickness correspond to defects on either the studied sample or the reference sample. The pixels corresponding to these artefacts

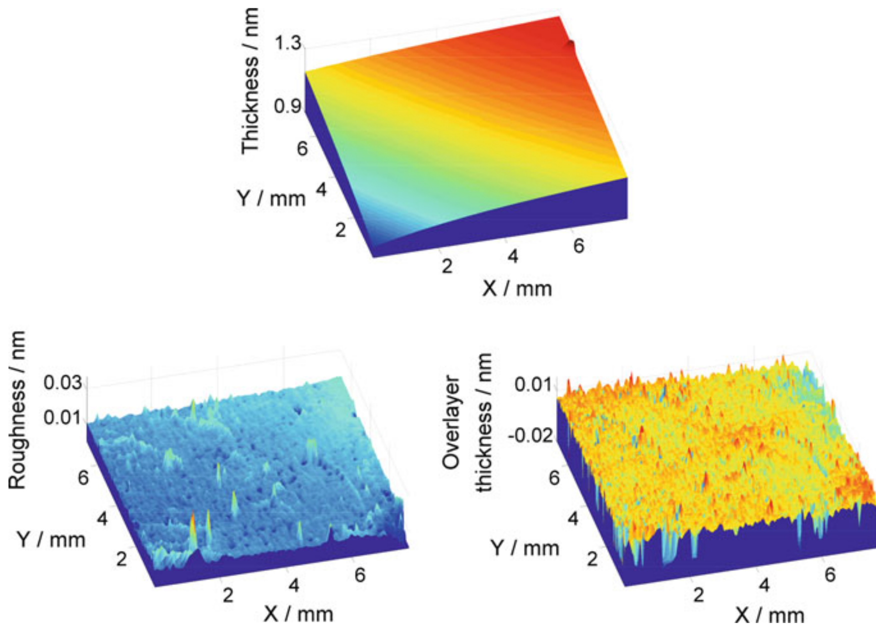

Fig. 5.17 Maps of local thickness of the ZnSe film, RMS roughness of its upper boundary and overlayer thickness

as well as bad pixels (with low quality of reflectance spectra) were removed, and the mean (or typical) values of the RMS roughness and overlayer thickness were determined from the remaining pixels.

The average RMS roughness of 4.7 nm agrees well with other optical [38, 49] and atomic force microscopy [38] studies. The average overlayer thickness value 10.3 nm is somewhat higher than the values found by other methods [38, 49] but still in reasonable agreement.

We can conclude that the ISR technique, when complemented by appropriate data processing approaches, is practical as a stand-alone method of optical characterization of thin films that differ significantly from ideal ones and which, therefore, require complex modeling.

5.9 Precision and Accuracy of ISR

At the beginning of this paragraph, it should be noted that the precision and accuracy of ISR depend, to a great extent, on the problem to be solved. In order to demonstrate the precision and accuracy of the ISR measurements themselves (i.e. the precision and accuracy of reflectance data obtained), a sample of a uniform SiO_2 film of the thickness of 800 nm was deposited on a Si substrate and then measured repeatedly

(eight times) by means of the reflectometer ISRER. All the reflectance data obtained in this manner were then compared with the theoretical values calculated by the method described in [56] using the values of the SiO_2 film optical constants obtained from many conventional measurements (VASE and SR, both in many configurations). This curve can be considered correct. The result can be seen in Fig. 5.18. In the top part of this figure, the theoretical curve is compared with the spectral dependence of the local reflectance of a selected small area of the film (imaged onto the relevant single pixel of the CCD camera) obtained by the ISR measurement. In the bottom half of the Fig. 5.18, each point of the graph represents the difference between the calculated theoretical curve at the given wavelength and the relevant mean value of the local reflectance acquired from all CCD pixels corresponding to a region located at the center of the measured sample. This region was selected to be approximately the same as the region utilized (i.e. illuminated) by the conventional techniques (VASE and SR). Different colors indicate different measurements. The relative mean difference was of about 5% in the vicinity of minima of the spectral reflectance dependencies. This value can be considered as the maximum relative difference between the correct and measured values of local thin film reflectance.

However, an ISR user is usually more interested in the reliability of determining sample optical parameter values rather than accuracy of individual reflectance values.

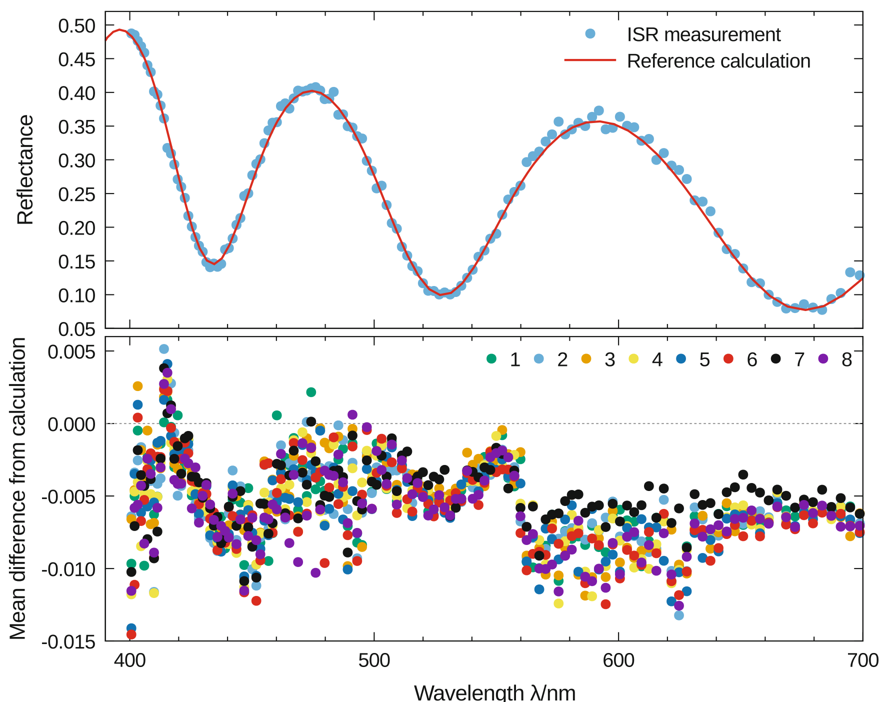

Fig. 5.18 Difference between measured ISRER spectra and theoretical reflectance curves

As it was mentioned in the conclusion of the Sect. 5.8.2, if the main task is to determine the local film thickness, the largest contribution to its error comes from the uncertainty of optical constants of the film material. Whether the optical constants are determined within ISR itself or taken from other measurements (and thus represent an external source of the error), they are seldom known with better accuracy than about 0.01. Consequently, as the technique is sensitive primarily to the optical thickness nh, the absolute thickness values are systematically deviated by a constant multiplicative factor. Depending on a film thickness and other aspects, this systematic deviation can reach up to a few nanometers. This point has to be considered in metrology, but it is moot in characterization of highly non-uniform samples in material research, where the spatial dependence (i.e. a shape) is more important. Therefore, we will further illustrate the precision of ISR results here as more relevant aspect.

Figure 5.19 illustrates the theoretical standard deviation of the thickness of a thin film (on a silicon substrate) determined from a typical ISRWS measurement. It represents the precision limit that cannot be improved without reducing noise or increasing the number of spectral points in a spectral dependence of the local reflectance of a film. The theoretical sensitivity of the measurement is apparently good, with the standard deviation of the fitted film thickness in tens of picometers.

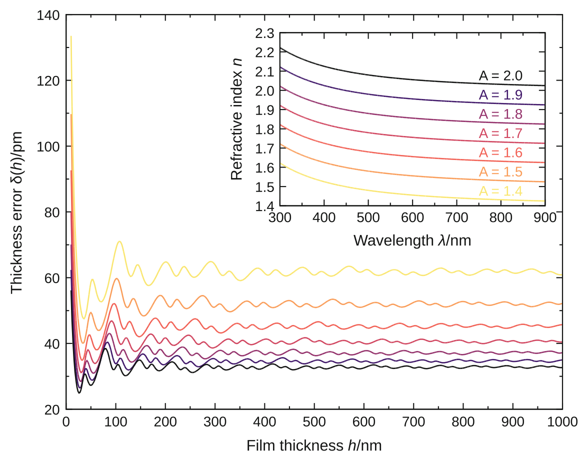

Fig. 5.19 Theoretical standard deviation of the fitted film thickness due to the noise for an ISRWS typical measurement, plotted as a function of film thickness and refractive index. Spectral dependencies of refractive index were modeled using a simple Cauchy formula; values of its constant term A are shown in the plot

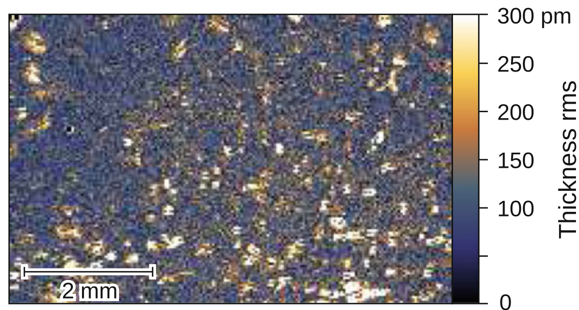

Fig. 5.20 Map of standard deviation of the fitted thickness of an 800 nm thick SiO_2 film obtained from repeated ISRWS measurement

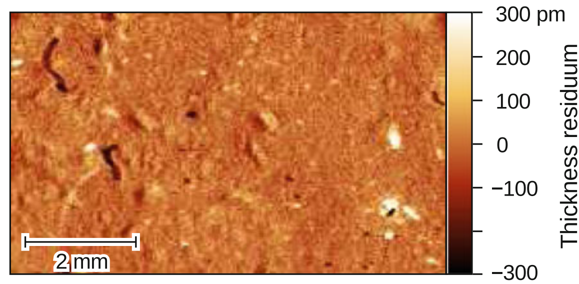

Fig. 5.21 Map of the residuum of fitted thickness of a 300 nm thick TiO_2 thin film (measured by ISRWS). The residuum was obtained by the subtraction of a low-level polynomial fitting the overall spatial dependence of thickness

To answer how does the theoretical estimate corresponds to actual experimental results, the above mentioned measurements of 800 nm thick SiO_2 film uniform in thickness were used. The individual measurements were independently fitted (with fixed optical constants) and the resulting thickness maps statistically analyzed. The map of the local standard deviation of fitted film thickness, which was obtained is shown in Fig. 5.20.

The film is rather uneven and contains spots with relatively large variation in the order of hundreds of picometers on the background of reproducible measurements. The overall mean and median of the map are 128 and 116 pm, respectively, less than twice the theoretical estimates. This verifies the good precision (reproducibility) also in practice.

Finally, Fig. 5.21 shows a complementary demonstration of the consistency of the ISR results. An almost uniform area of a 300 nm thick TiO_2 thin film was measured and the map fitted (with fixed optical constants). Since the uniformity was not perfect, the thickness map was then fitted with a low-order polynomial, and the polynomial subtracted to obtain the residuum plotted in Fig. 5.21. In the ideal case, the residuum would be zero. The map again contains isolated spots where the residuum is of the order of hundreds of picometers. However, the mean square residuum is 52 pm, i.e. about twice the theoretical value (TiO_2 has a much higher refractive index).

5.10 Another Application of ISR

Up to now, we have focused on the ISR application to the basic task of the optical characterization of thin films, i.e. determination of their thickness and spectral dependencies of their optical constants. These films could exhibit some defects like thickness non-uniformity, non-uniformity in upper boundary roughness and their structural model could comprise an overlayer. The ability to measure spatially resolved reflectance in a wide spectral range can be beneficial also in other applications. As an example of such an application can serve the use of ISR for the localization of metallic gold in an organic layer. The metallic gold was reduced from an organo-metallic compound by a localized thermal treatment using a plasma-jet [57]. The plasma treatment of solid surfaces has a lot of interesting and important applications generally. In

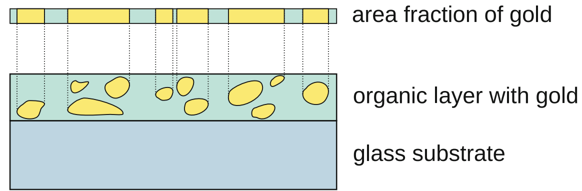

Fig. 5.22 The organogold layer with reduced grains of gold. Grain projection on the film surface is shown

the application mentioned above organogold layers were prepared on a microscopy glass plate by spincoating and then vacuum dried (the detailed description of the layers preparation see [57]).

In these layers, the gold was in the oxidation state +1. By the action of plasma jet, this gold contained in the precursor layers is reduced to metallic gold (i.e. gold in its oxidation state 0) in the form of small grains (see Fig. 5.22).

The projection of these metallic gold grains on the layer surface can be quantitatively evaluated by means of the ISR technique. The models used for the description of light interaction with the studied layers can be various. They have to respect the fact that the layers of interest are approximately 6 µm thick, non-uniform and the refractive index of their organic material is close to that of the glass substrate. Hence, the interference of light is weak in those parts, where the layers are transparent. The parts with metallic gold (the heat treated parts) were not transparent. Therefore, the layers were modeled as thick slabs and the interference was not considered. It was also taken into account that the layers significantly differ from ideal ones, which implies various defects and distortions in the reflectance spectra. Considering also a huge number of ISR experimental data, a simple, robust, model was needed which would agree with experimental data as much as possible. Finally, the layer was modeled as a thick slab formed by separated regions covered by the untreated organic compound or metallic gold. This model works with an area fraction of metallic gold a_f, which is defined as follows:

$$a_f^{u,v} = \frac{A_{gold}^{u,v}}{A_{reg}^{u,v}}.$$

The area of gold covering the region corresponding to a camera pixel (with coordinates u and v) is denoted as $A_{gold}^{u,v}$ and $A_{reg}^{u,v}$ is the area of this whole region. Using $a_f^{u,v}$, the local relative reflectance of the region corresponding to the same CCD camera pixel can be expressed as

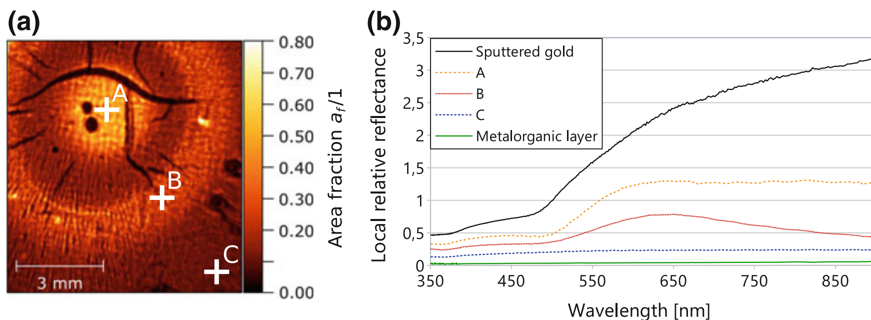

Fig. 5.23 **a** Area metallic gold map obtained by ISR measurements. The scale shows a value of the model parameter a_f–the area fraction of metallic gold in the organogold precursor treated by plasma jet. **b** Local relative reflectance comparison. Measured local relative reflectance of the spots (marked in a) on the measured sample together with measurements of the pure gold layer and the organogold layer without any plasma jet treatment

$$R^{u,v}(\lambda_k) = a_f^{u,v} R_{gold}(\lambda_k) + (1 - a_f^{u,v}) R_{org}(\lambda_k). \tag{5.4}$$

Here, $R_{gold}(\lambda_k)$ is the value of the relative reflectance of gold obtained by measuring the reference sample (a uniform gold layer prepared by magnetron sputtering on a glass sheet) at the wavelength λ_k. $R_{org}(\lambda_k)$ is the value of the relative reflectance of the untreated uniform organogold precursor layer at the same wavelength. The values of $a_f^{u,v}$ were determined by the least square method using the previous equation (5.4). Put together, these values form a map of the area projection of the reduced metallic gold distribution in the studied sample.

The results achieved are shown in Fig. 5.23a. Three spots A, B, C are selected in this figure to illustrate how the corresponding local relative reflectance obtained by the ISR is changing along the surface of the studied film (see Fig. 5.23b). The spot A contains the largest amount of metallic gold (and thus its reflectance is closest to pure metallic gold), the spot B contains less metallic gold and the spot C was not thermally treated and thus it does not contain any metallic gold.

The ISR method was completed by X-ray photoelectron spectroscopy applied at the points A, B, C of the sample surface and confocal microscopy (which provides only qualitative evaluation of the area distribution of metallic gold along the studied sample surface). Results obtained by means of both the additional techniques were consistent with the quantitative results from ISR.

5.11 Conclusion

In the deposition of thin films for optical applications, various factors may cause defects significantly affecting the desired properties of these films. This is valid particularly during the development and tuning of a new deposition technology. Therefore, it is desired to have instruments which can detect the existence of these defects and characterize the influence of them on thin film optical properties. The ISR technique, in conjunction with the adequate data processing methods, is such a suitable tool for this purpose. The advantages of the ISR fully manifest when characterizing thin films with area non-uniformity in their parameters. When such a non-uniformity is of a general type, i.e. it is not possible to describe this non-uniformity analytically, a correct optical characterization of these films by means of the conventional (non-imaging) and frequently used optical methods (e.g. photometric and ellipsometric methods) cannot be performed.

The main aim of ISR in the field of thin film optics is the determination of thin film optical parameters, primarily maps of local thickness, and spectral dependencies of optical constants. With the help of ISR, it is also possible to determine other material parameters appearing in the dispersion models, such as the band gap of a thin film material, the maximum energy limit of the relevant electron transitions, or a quantity proportional to the concentration of electrons participating in the transitions. Eventually, it also allows to determine some structural parameters, such as maps of local RMS roughness of the upper film boundary.

The experimental set up of the ISR technique is simple. The design of imaging spectroscopic reflectometers allows to measure thin film samples up to 20 mm × 20 mm size, at normal angle of light incidence. The measurements can be done within the spectral range (270–1000) nm, i.e. (1.2–4.6) eV, with the spatial resolution on the sample up to 16 μm × 16 μm and the maximum value of the local thickness gradient approximately 12.5 μm/mm. The duration of a one sample measurement is typically 30 min (without the measurement of the reference sample and the background, which need not to be measured every time).

The ISR technique provides a tremendous amount of experimental data. This fact implies the necessity of special data processing methods with the aim to determine the sought optical parameters of the film. The use of the appropriate method is determined by a task to be solved. If spectral dependence of optical constants of a thin film is known, the stand-alone single-pixel ISR method can be used for the determination of the map of the film local thickness. If the spectral dependence of optical constants of a thin film is not known, conventional (non-imaging) methods can be used for their determination under the assumption of film uniformity in these constants. The single-pixel ISR method can then be used for the determination of the map of the local thickness of the film as a complementary method. The same task can be solved using the stand-alone manual multi-pixel ISR method.

The multi-pixel approach is equivalent to the multi-sample approach which is inherently present in the ISR technique. This fact further increases the efficiency of this method in solving the basic task of spectroscopic reflectometry. The most

powerful ISR method is the global ISR method which enables to address the issue of the characterization of a thin film which is even far from an ideal one. That is, it enables us to determine the unknown spectral dependence of thin film optical constants (assuming the uniformity of the film in optical constants), the map of thin film local thickness and, if necessary, other parameters of the film, such as the RMS roughness of the upper boundary and the mean thickness of the overlayer film. This global method uses an original algorithm for processing the ISR data, which ensures fast convergence of the procedure finding the sought thin film parameters. The above-mentioned ISR technique and the ISR methods form an integral whole – ISR.

It is necessary to mention that all the ISR methods presented here are built on the assumption of thin film uniformity in optical constants. In accordance with our experience, this assumption is fulfilled in the vast majority of real-life cases. In principle, the characterization of thin films exhibiting non-uniformity in optical constants and simultaneously in thickness is also possible using ISR. However, up to date this task still represents a challenge.

The accuracy of optical parameters determined by means of ISR depends on the concrete issue that is being addressed. The optical constants can be seldom determined with a better accuracy than about 0.01. The uncertainty of optical constants causes a systematic deviation of the local thickness of the measured thin film. Depending on the film thickness and other aspects, this systematic deviation can even be a few nanometers. The precision of ISR measurements is good. In the case of the local thickness determination, this precision can be estimated by the value of the RMS deviation in the local thickness which is in the order of 10^1–10^2 picometers.

The applicability range of ISR can be defined as follows: Since the aim of applying the ISR technique is, among other things, to determine a map of the thin film local thickness, it is necessary to exploit the interference pattern which originated in the film. This means there must be interaction between the light beam and the bottom boundary of the film, which affects the local reflection of the film. Thus, only thin films that absorb sufficiently little in the spectral range used can be studied by means of the ISR technique. By other words, the ISR technique can be utilized for dielectric or semiconductor thin films, but not for strongly absorbing thin films (e.g. metal films).

In the previous paragraphs, we dealt with the application of ISR within the field of optical characterization of thin films. We presented not only a solution of the basic task of finding the spectral dependence of optical constants and determination of local thickness maps of thin films, but also pointed out a wider potential of ISR in this field (see Sect. 5.10). Generally speaking, ISR can also be a good choice for the analysis of intentionally modified thin films (like are patterned, locally deposited, locally etched films). In conclusion, we can state that ISR represents the powerful tool for optical characterization of thin films. At the same time, it should be noted that the potential for using ISR outside the thin film optics field is also high. It can be successfully applied wherever it is desirable to know the local reflectance maps along the surface of the studied samples, such as biological, medical objects, etc.

Acknowledgements The work on this chapter was supported by the project LO1411 (NPU I) funded by Ministry of Education Youth and Sports of the Czech Republic. Presented reflectometers were realized using the facilities of Institute of Physical Engineering, Brno University of Technology.

References

1. H.G. Tompkins, W.A. McGahan, *Spectroscopic Ellipsometry and Reflectometry: A User's Guide* (Wiley, 1999). Google-Books-ID: W35tQgAACAAJ
2. H.G. Tompkins, E.A. Irene, *Handbook Of Ellipsometry* (William Andrew Publisher; Springer, Norwich, NY; Heidelberg, Germany, 2005). http://www.books24x7.com/marc.asp?bookid=32277. OCLC: 310147997
3. M. Quinten, *A Practical Guide to Optical Metrology for Thin Films* (Wiley-VCH Verlag GmbH & Co, KGaA, 2012)
4. M.I. Török, Optica Acta: Int. J. Opt. **32**(4), 479 (1985). https://doi.org/10.1080/713821745
5. T. Pisarkiewicz, T. Stapinski, H. Czternastek, P. Rava, J. Non-Cryst. Solids **137**, 619 (1991). https://doi.org/10.1016/S0022-3093(05)80194-2, http://www.sciencedirect.com/science/article/pii/S0022309305801942
6. T. Pisarkiewicz, J. Phys. D: Appl. Phys. **27**(1), 160 (1994). https://doi.org/10.1088/0022-3727/27/1/025, http://stacks.iop.org/0022-3727/27/i=1/a=025
7. E. Márquez, J.M. González-Leal, R. Jiménez-Garay, S.R. Lukic, D.M. Petrovic, J. Phys. D: Appl. Phys. **30**(4), 690 (1997). https://doi.org/10.1088/0022-3727/30/4/026, http://stacks.iop.org/0022-3727/30/i=4/a=026
8. E. Márquez, P. Nagels, J.M. González-Leal, A.M. Bernal-Oliva, E. Sleeckx, R. Callaerts, Vacuum **52**(1–2), 55 (1999). https://doi.org/10.1016/S0042-207X(98)00233-4, http://www.sciencedirect.com/science/article/pii/S0042207X98002334
9. D. Nečas, I. Ohlídal, D. Franta, J. Opt. A: Pure Appl. Opt. **11**(4), 045202 (2009). https://doi.org/10.1088/1464-4258/11/4/045202, http://iopscience.iop.org/1464-4258/11/4/045202
10. L. Abel-Tiberini, F. Lemarquis, M. Lequime, Appl. Opt. **45**(7), 1386 (2006). https://doi.org/10.1364/AO.45.001386
11. D. Nečas, I. Ohlídal, D. Franta, V. Čudek, M. Ohlídal, J. Vodák, L. Sládková, L. Zajíčková, M. Eliáš, F. Vižd'a, Thin Solid Films **571**, Part 3, 573 (2014). https://doi.org/10.1016/j.tsf.2013.12.036
12. J. Spousta, M. Urbánek, R. Chmelík, J. Jiruše, J. Zlámal, K. Navrátil, A. Nebojsa, T. Šikola, Surf. Interface Anal. **34**(1), 664 (2002). https://doi.org/10.1002/sia.1383, http://onlinelibrary.wiley.com/doi/10.1002/sia.1383/abstract
13. M. Urbánek, J. Spousta, K. Navrátil, R. Szotkowski, R. Chmelík, M. Buček, T. Šikola, Surf. Interface Anal. **36**(8), 1102 (2004). https://doi.org/10.1002/sia.1850, http://onlinelibrary.wiley.com/doi/10.1002/sia.1850/abstract
14. I. Ohlídal, D. Nečas, D. Franta, V. Buršíková, Diam. Relat. Mater. **18**(2–3), 364 (2009). https://doi.org/10.1016/j.diamond.2008.09.003, http://www.sciencedirect.com/science/article/pii/S0925963508004342
15. D. Nečas, D. Franta, V. Buršíková, I. Ohlídal, Thin Solid Films **519**(9), 2715 (2011). https://doi.org/10.1016/j.tsf.2010.12.065
16. D. Nečas, I. Ohlídal, D. Franta, J. Opt. **13**(8), 085705 (2011). https://doi.org/10.1088/2040-8978/13/8/085705, http://stacks.iop.org/2040-8986/13/i=8/a=085705
17. L. Stiblert, T. Sandström, Le J. de Phys. Colloq. **44**(C10) (1983). https://doi.org/10.1051/jphyscol:19831016
18. D. Beaglehole, Review of Scientific Instruments **59**(12), 2557 (1989). https://doi.org/10.1063/1.1139897
19. G. Jin, P. Tengvall, I. Lundström, H. Arwin, *Analytical Biochemistry* (1995), p. 69. https://doi.org/10.1006/abio.1995.9959

20. H. Arwin, Thin Solid Films **313–314**, 764 (1998). https://doi.org/10.1016/S0040-6090(97)00993-0, http://www.sciencedirect.com/science/article/pii/S0040609097009930
21. L. Asinovski, D. Beaglehole, M.T. Clarkson, phys. status solidi (a) **205**(4), 764 (2008). https://doi.org/10.1002/pssa.200777855, http://onlinelibrary.wiley.com/doi/10.1002/pssa.200777855/abstract
22. U. Wurstbauer, C. Röling, U. Wurstbauer, W. Wegscheider, M. Vaupel, P.H. Thiesen, D. Weiss, Appl. Phys. Lett. **97**(23), 231901 (2010). https://doi.org/10.1063/1.3524226, http://scitation.aip.org/content/aip/journal/apl/97/23/10.1063/1.3524226
23. M. Fried, G. Juhász, C. Major, P. Petrik, O. Polgár, Z. Horváth, A. Nutsch, Thin Solid Films **519**(9), 2730 (2011). https://doi.org/10.1016/j.tsf.2010.12.067, http://www.sciencedirect.com/science/article/pii/S0040609010016974
24. G. Jin, Y.H. Meng, L. Liu, Y. Niu, S. Chen, Q. Cai, T.J. Jiang, Thin Solid Films **519**(9), 2750 (2011). https://doi.org/10.1016/j.tsf.2010.12.175, http://www.sciencedirect.com/science/article/pii/S0040609010018249
25. P.G. Ellingsen, M.B. Lilledahl, L.M.S. Aas, C.d.L. Davies, M. Kildemo, J. Biomed. Opt. **16**(11), 116002 (2011). https://doi.org/10.1117/1.3643721
26. K. Mahmoud, S. Park, S.N. Park, D.H. Lee, Metrologia **51**(6), S293 (2014). https://doi.org/10.1088/0026-1394/51/6/S293. WOS:000345426000008
27. K. Mahmoud, S. Park, S.N. Park, D.H. Lee, in *Fifth Asia-Pacific Optical Sensors Conference*, vol. 9655, ed. by B. Lee, S.B. Lee, Y. Rao (Spie-Int Soc Optical Engineering, Bellingham, 2015), vol. 9655, p. 965503. WOS:000358602400002
28. K. Kim, S. Kim, S. Kwon, H.J. Pahk, Int. J. Precis. Eng. Manuf. **15**(9), 1817 (2014). https://doi.org/10.1007/s12541-014-0534-3
29. M. Ohlídal, I. Ohlídal, D. Franta, T. Králík, M. Jákl, M. Eliáš, Surf. Interface Anal. **34**(1), 660 (2002). https://doi.org/10.1002/sia.1382, http://onlinelibrary.wiley.com/doi/10.1002/sia.1382/abstract
30. M. Ohlídal, I. Ohlídal, P. Klapetek, M. Jákl, V. Čudek, M. Eliáš, Jpn. J. Appl. Phys. **42**(7S), 4760 (2003). https://doi.org/10.1143/JJAP.42.4760, http://iopscience.iop.org/1347-4065/42/7S/4760
31. I. Ohlídal, M. Ohlídal, P. Klapetek, V. Čudek, M. Jákl, in *Wave-Optical Systems Engineering II* (2004), pp. 260–271. https://doi.org/10.1117/12.509628, http://dx.doi.org/10.1117/12.509628
32. M. Ohlídal, V. Čudek, I. Ohlídal, P. Klapetek, in *Proceedings of SPIE*, ed. by C. Amra, N. Kaiser, H.A. Macleod (2005), vol. 5963, pp. 596, 329–596, 329–9. https://doi.org/10.1117/12.625380, http://proceedings.spiedigitallibrary.org/proceeding.aspx?articleid=876920
33. M. Ohlídal, I. Ohlídal, P. Klapetek, D. Nečas, V. Buršíková, Diam. Relat. Mater. **18**(2–3), 384 (2009). https://doi.org/10.1016/j.diamond.2008.10.012
34. M. Ohlídal, I. Ohlídal, E-J. Surf. Sci. Nanotechnol. **7**, 409 (2009). https://doi.org/10.1380/ejssnt.2009.409
35. I. Ohlídal, M. Ohlídal, D. Nečas, D. Franta, V. Buršíková, Thin Solid Films **519**(9), 2874 (2011). https://doi.org/10.1016/j.tsf.2010.12.069, http://ww.sciencedirect.com/science/article/pii/S0040609010016998
36. M. Ohlídal, I. Ohlídal, P. Klapetek, D. Nečas, A. Majumdar, Meas. Sci. Technol. **22**(8), 085104 (2011). https://doi.org/10.1088/0957-0233/22/8/085104, http://iopscience.iop.org/0957-0233/22/8/085104
37. D. Nečas, V. Čudek, J. Vodák, M. Ohlídal, P. Klapetek, J. Benedikt, K. Rügner, L. Zajíčková, Meas. Sci. Technol. **25**(11), 115201 (2014). https://doi.org/10.1088/0957-0233/25/11/115201
38. D. Nečas, I. Ohlídal, D. Franta, M. Ohlídal, V. Čudek, J. Vodák, Appl. Opt. **53**(25), 5606 (2014). https://doi.org/10.1364/AO.53.005606
39. J. Schaefer, J. Hnilica, J. Sperka, A. Quade, V. Kudrle, R. Foest, J. Vodak, L. Zajickova, Surf. Coat. Technol. **295**, 112 (2016). https://doi.org/10.1016/j.surfcoat.2015.09.047. WOS:000376834700017
40. D. Nečas, I. Ohlídal, D. Franta, M. Ohlídal, J. Vodák, J. Opt. **18**(1), 015401 (2016). https://doi.org/10.1088/2040-8978/18/1/015401, http://stacks.iop.org/2040-8986/18/i=1/a=015401

41. J. Vodák, D. Nečas, M. Ohlídal, I. Ohlídal, Measurement Science and Technology **28**(2), 025205 (2017). https://doi.org/10.1088/1361-6501/aa5534, http://stacks.iop.org/0957-0233/28/i=2/a=025205
42. P. Hariharan, *Optical Interferometry* (Academic Press, 2003). Google-Books-ID: EGdMO3rfVj4C
43. D. Franta, I. Ohlídal, Acta Phys. Slovaca **50**(4), 411 (2000)
44. A. Majumdar, J. Schäfer, P. Mishra, D. Ghose, J. Meichsner, R. Hippler, Surf. Coat. Technol. **201**(14), 6437 (2007). https://doi.org/10.1016/j.surfcoat.2006.12.011, http://www.sciencedirect.com/science/article/pii/S0257897206014800
45. D. Franta, D. Nečas, L. Zajíčková, Opt. Express **15**(24), 16230 (2007). https://doi.org/10.1364/OE.15.016230, https://www.osapublishing.org/oe/abstract.cfm?uri=oe-15-24-16230
46. D. Franta, D. Nečas, L. Zajíčková, I. Ohlídal, Thin Solid Films **571**, 490 (2014). https://doi.org/10.1016/j.tsf.2014.03.059
47. D. Nečas, J. Vodák, I. Ohlídal, M. Ohlídal, A. Majumdar, L. Zajíčková, Appl. Surf. Sci. **350**, 149 (2015). https://doi.org/10.1016/j.apsusc.2015.01.093, http://www.sciencedirect.com/science/article/pii/S016943321500118X
48. V. Holý, K. Wolf, M. Kastner, H. Stanzl, W. Gebhardt, J. Appl. Crystallogr. **27**(4), 551 (1994). https://doi.org/10.1107/S0021889894000208, http://scripts.iucr.org/cgi-bin/paper?wi0141
49. D. Franta, I. Ohlídal, P. Klapetek, A. Montaigne-Ramil, A. Bonanni, D. Stifter, H. Sitter, J. Appl. Phys. **92**(4), 1873 (2002). https://doi.org/10.1063/1.1489068, http://aip.scitation.org/doi/10.1063/1.1489068
50. D. Franta, D. Nečas, L. Zajíčková, Thin Solid Films **534**, 432 (2013). https://doi.org/10.1016/j.tsf.2013.01.081
51. D. Franta, D. Nečas, L. Zajíčková, I. Ohlídal, J. Stuchlík, D. Chvostová, Thin Solid Films **539**, 233 (2013). https://doi.org/10.1016/j.tsf.2013.04.012
52. I. Ohlídal, D. Necas, D. Franta, phys. status solidi (c) **5**(5), 1399 (2008). https://doi.org/10.1002/pssc.200777769, http://onlinelibrary.wiley.com/doi/10.1002/pssc.200777769/abstract
53. J.A. Ogilvy, H.M. Merklinger, J. Acoust. Soc. Am. **90**(6), 3382 (1991). https://doi.org/10.1121/1.401410, http://asa.scitation.org/doi/abs/10.1121/1.401410
54. D. Franta, I. Ohlídal, P. Klapetek, A. Montaigne-Ramil, A. Bonanni, D. Stifter, H. Sitter, Acta Phys. Slovaca **53**(2), 95 (2003)
55. S. Adachi, *Optical properties of crystalline and amorphous semiconductors: materials and fundamental principles* (Boston: Kluwer Academic Publishers, 1999). http://trove.nla.gov.au/version/39699241
56. D. Franta, D. Nečas, I. Ohlídal, A. Giglia, in *Optical Systems Design 2015: Optical Fabrication, Testing, and Metrology V*, vol. 9628 (2015), vol. 9628, pp. 96,281U–96,281U–12. https://doi.org/10.1117/12.2190104
57. J. Vodák, D. Nečas, D. Pavliňák, J.M. Macak, T. Řičica, R. Jambor, M. Ohlídal, Appl. Surf. Sci. **396**, 284 (2017). https://doi.org/10.1016/j.apsusc.2016.10.122